

Study of a 0.35 THz Extended Interaction Oscillator Driven by a Pseudospark-Sourced Sheet Electron Beam

Jie Xie, Liang Zhang, Huabi Yin, Wenlong He, Kevin Ronald, A. D. R. Phelps, Xiaodong Chen, Jin Zhang, Yasir Alfadhli, Xuesong Yuan, Lin Meng and Adrian W. Cross

Abstract—A compact high power extended interaction oscillator (EIO) driven by a pseudospark-sourced (PS-sourced) sheet electron beam is presented at 0.35 THz. It combines the advantages of a planar interaction circuit and a sheet electron beam generated from the PS discharge, including a large beam cross section, high gain per unit length, high current density with the additional benefit of not requiring an external focusing magnetic field. Staying within what is achievable with microfabrication techniques, the influence of tolerance on the Q-value, resonance frequency, and characteristic impedance was investigated. The effect of surface roughness caused by the manufacturing method on Ohmic loss of the material surface was studied. The advanced microfabrication techniques of UV-LIGA and Nano-CNC which are capable of realizing high precision and a metal surface of sufficient smoothness, were proposed to manufacture the planar structures. The effect of plasma density in PS-sourced sheet electron beam on the resonance frequency of the EIO circuit was investigated. The simulation results showed that the output signal had a slight frequency upshift and a decrease of the output power as the plasma density increased at 0.35 THz, which is consistent with the theoretical analysis. Beam-wave interaction simulations for this planar EIO predicted a peak output power of 1.8 kW at ~0.35 THz using an effective value of conductivity of 1.1×10^7 S/m to take into account the skin depth and surface roughness.

Index Terms—Extended interaction oscillator (EIO), high power radiation, pseudospark-sourced electron beam, sheet electron beam, terahertz.

This work was supported by the UK Engineering and Physical Sciences Research Council (EPSRC) under Grants EP/S00968X/1 and EP/S009582/1. Jie Xie thanks the support from the National Key Research and Development Program of China (No.2019YFA0210202), National Natural Science Foundation of China (No.61771096) and Fundamental Research Funds for the Central Universities (No.ZYGX2019J012, No.ZYGX2019Z006). (Corresponding author: Jie Xie)

Jie Xie, Xuesong Yuan, and Lin Meng are with the Vacuum Electronics National Laboratory, School of Electronic Science and Engineering, University of Electronic Science and Technology of China, Chengdu 610054, China, and Jie Xie is also with the Department of

I. Introduction

HIGH power millimeter-wave (MMW) and terahertz (THz) (0.1-3THz) radiation sources have increasing prominence in numerous exciting applications such as broadband wireless and high data rate communication, ultra-narrow pulse generation for UWB radar, imaging and biological spectroscopy, biomedical and plasma diagnostics [1-6]. Compared with solid-state semiconductor devices, the vacuum electron devices (VEDs) have the advantages of high output power and robustness therefore they remain the first-choice for high-power MMW and terahertz sources. However, increasing the operating frequency to the THz region of the electromagnetic spectrum, the dimension of the device decreases dramatically, which results in a significant reduction in cathode current. Increasing the electron emission current density is a potential solution, however, it is challenging for the thermionic cathode which has a current density typically less than 100 A/cm^2 [1, 7, 8]. The pseudospark (PS) discharge system can produce a high-intensity electron beam pulse with beam current density up to 10^4 A/cm^2 and brightness up to $10^{12} \text{ A/(m}^2\text{-rad}^2)$ [9-12]. It also benefits from the unique self-focusing due to the ion channel generated by the beam front, the microwave radiation sources based on a PS discharge can transport a high current beam without the need of an external magnetic field. A typical four-gap PS discharge setup is shown in Fig. 1. Its structure consists of a hollow cathode (HC) with a central hole in the anode. The generated electron beam can be extracted through a hollow hole on the anode. The HC and anode are separated by one or more insulators. Microwave devices based on the PS-sourced electron beam have been experimentally studied covering various frequency bands, such as a Cherenkov maser operating at Ka-band [13], a X-band

Physics, University of Strathclyde, Glasgow, G4 0NG, U.K. (e-mail: jet.jiexie@gmail.com).

L. Zhang, H. Yin, A. W. Cross, and A. D. R. Phelps are with the Department of Physics, University of Strathclyde, Glasgow, G4 0NG, U.K. (e-mail: a.w.cross@strath.ac.uk).

Wenlong He is with the College of Electronic Science and Technology, Shenzhen University, Shenzhen, 518060, China (email: wenlong.he@szu.edu.cn).

Xiaodong Chen, Jin Zhang, and Yasir Alfadhli are with the School of Electronic Engineering and Computer Science, Queen Mary University of London, London E1 4NS, U.K. (xiaodong.chen@qmul.ac.uk).

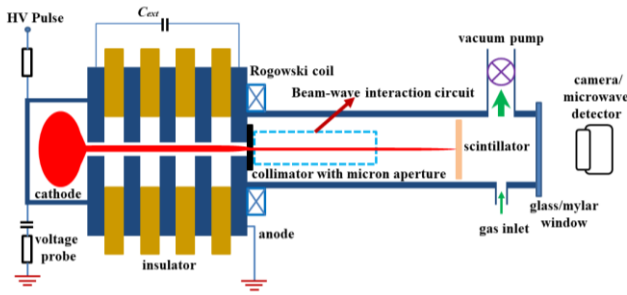


Fig. 1. A four-gap PS-sourced electron beam experimental setup.

slow-wave oscillator [14], EIOs operating at W-band and G-band [11, 15-17], and a backward wave oscillator (BWO) operating at G-band [10].

The EIO is one of the VEDs that can achieve reliable output with high power, high interaction efficiency, and reasonable bandwidth at MMW and THz frequencies [17-21]. The interaction structure consists of multiple interaction gaps, which avoids the breakdown and raises the cavity impedance, contributing to the production of high power coherent radiation. At THz frequencies, the Ohmic loss increases greatly. High gain per unit length produces a short interaction circuit, which helps to reduce the Ohmic loss. EIOs driven by thermionic cathodes have been demonstrated in the sub-millimeter

Symbol	Description	Value
p	Period length	0.269 mm
d	Gap length	0.110 mm
gy	Gap height	0.485 mm
gx	Gap width	1.100 mm
cy	Cavity height	0.577 mm
cx	Cavity width	0.342 mm

(FELs). In the experiment, a PS electron beam current of 118 A was measured after propagating through a 60 mm long collimator of diameter 3.5 mm in diameter [29]. At a smaller collimator diameter of 0.07 mm, a beam current of 50 mA was measured 20 cm downstream of the anode [10].

A sheet electron beam (SEB) has the advantage of less space charge effect and large interaction current as compared to a cylindrical system, which helps to increase the output power. However, it is challenging to generate a SEB from a thermionic cathode as a complicated magnetic guiding system is required. It is much simpler in a PS system to use a collimator with a rectangular aperture placed at the end of the anode and keep the rest of the system unchanged. In the experiment a PS sheet electron beam (PS-SEB) with a peak current of 21.5 A and

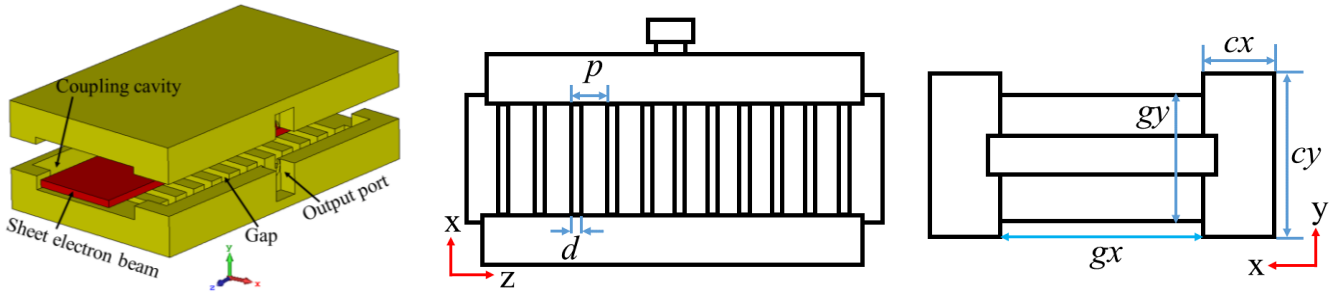


Fig. 2. Schematic drawing of the EIO circuit with eleven-slot: 3D and cross-section views.

frequency range. A continuous wave power performance of 5 W has been established at 263 GHz by CPI Canada [20]. However, as the frequency increases, the miniature circuit dimensions restrict the provision of high current, and Ohmic losses increase rapidly.

In this paper, an EIO operating at 352 GHz driven by a PS-sourced electron beam was studied. Apart from the benefit of high current density from the PS-sourced beam, a sheet electron beam (SEB) was chosen to further enlarge the cross-section of beam-wave interaction and reduce the space charge effect.

II. PS-SOURCED SHEET ELECTRON BEAM

The PS discharge is a low pressure (typically in the range of 20 to 200 mTorr) gas discharge in an axially symmetric structure. It was first experimentally studied by Christiansen and Schultheiss in the late 1970's [22]. A self-sustained electron beam pulse can be produced with high-brightness, low emittance ($\sim 15 \text{ mm} \cdot \text{mrad}$), small beam diameter ($< 4 \text{ mm}$), and fast current rise (up to 10^{12} A/s), as well as high beam current density ($\sim 10^8 \text{ A/m}^2$) [23-28], which is catered to the requirement for high power sources of millimeter-wave and THz radiation, such as BWOs, EIOs, free-electron lasers

34.5 kV peak voltage was measured without an external focusing magnetic field using a post-acceleration modulator where the cross section dimension of the SEB was $1.0 \text{ mm} \times 0.17 \text{ mm}$ [17]. In this paper, the PS generated SEB will be used to drive a 0.35 THz EIO structure.

III. DESIGN AND SIMULATION OF PS-SEB EIO

EIO combines the advantages of travelling wave tubes and klystrons [20, 30]. It is known for its high power, high efficiency, and there can be some limited tuning in the millimeter wave and THz regime. The interaction circuit composes of eleven resonant slots as shown in Fig 2. The slow-wave structure (SWS) is strongly coupled by symmetrical coupling cavities on both sides of the structure. A $1.3 \text{ mm} \times 0.18 \text{ mm}$ rectangular beam tunnel passes through the center of the slots and intersects with the SWS. The extended cavity improves the coupling impedance of the cavity enabling efficient modulation of the electron beam across a broad frequency band. By distributing the electric field across several gaps within a single cavity, it helps to reduce the gap voltage to avoid breakdown and arcing.

According to the synchronous condition of the EIO, the

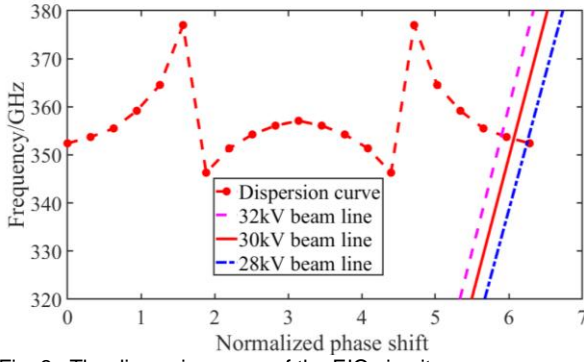


Fig. 3. The dispersion curve of the EIO circuit.

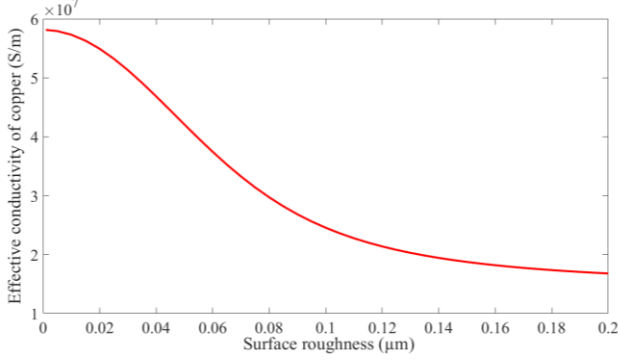


Fig. 4. The relationship between surface roughness and effective conductivity of copper.

period length p of the multi-gap cavity is [31]

$$\beta_e p = m\pi \quad (1)$$

$$\beta_e = 2\pi f / v_e \quad (2)$$

$$v_e = c \cdot \sqrt{1 - \frac{1}{\left(1 + \frac{U}{511}\right)^2}} \quad (3)$$

Where β_e , v_e , U , c , and f are the propagation constant of the electron beam, the beam velocity and voltage, the speed of light and the resonant frequency, respectively. Unlike the single gap cavity, the SWS has multiple eigenmodes in the pass-band. Among these eigenmodes, the 2π mode ($m=2$) was chosen as the operating mode to maximize the cavity impedance at the passband cut-offs. The velocity of the electron beam was chosen so that the traveling time between the adjacent gap was equal to the period of the electromagnetic wave supported by the SWS to ensure an effective beam-wave interaction. The optimal dimensions of a structure operating at a frequency of about 352 GHz, with a 28-kV beam voltage and a $1.3 \text{ mm} \times 0.18 \text{ mm}$ rectangular beam tunnel, were achieved by parameter sweeps and are listed in Table I. The dispersion curve illustrated in Fig. 3 is an effective approach to identify the possible mode competitions and self-oscillation. The beam lines at beam voltages of 28, 30, and 32 kV are also plotted in Fig. 3. When the voltage reaches 31 kV, the adjacent competition mode ($1/11\pi$) will dominate. The voltage dynamic tuning range is about 3 kV from 28 kV to 31 kV.

A. Analysis of Ohmic Loss and Effects of Tolerance Fabrication

The Ohmic loss on copper varies with the surface roughness. The non-ideal surface losses at THz frequencies caused by surface roughness have been reported [32]. The Hammerstad-

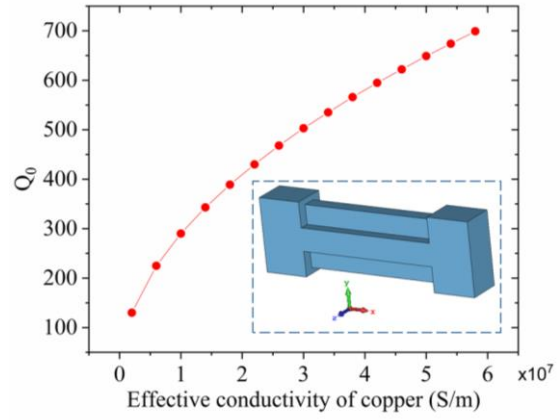


Fig. 5. Simulation results for Q_0 versus effective conductivity of copper in single cavity.

Bekkadal formula can be used to predict the excess resistive loss caused due to a rough metallic surface:

$$\sigma_{eff} = \sigma_0 \cdot \left\{ 1 + \frac{2}{\pi} \arctan \left[1.4 \left(\frac{h}{\delta} \right)^2 \right] \right\}^{-2} \quad (4)$$

Here, σ_0 is the conductivity of the ideal metal surface ($\sigma_{Cu} = 5.8 \times 10^7 \text{ S/m}$ for copper), σ_{eff} is the effective conductivity of the rough surface, δ is the skin depth in the case of an ideal metal, and h is the RMS height of the surface. Fig. 4 shows the relationship between the surface roughness and the effective conductivity of copper at 353 GHz. The surface Ohmic loss is a significant issue with regard to the fabrication of the interaction circuit. To reduce the power loss caused by surface resistance, the surface roughness should be smaller than the skin depth of the 353 GHz submillimeter wave signal, approximately 110 nm for copper. Fig. 5 shows the simulation results for the intrinsic quality factor Q_0 versus effective conductivity of copper in a single cavity using 3D EM simulation code CST Microwave Studio. At a high frequency of 353 GHz, a high-quality factor is difficult to achieve due to the large Ohmic loss. According to eq. 4, surface roughness of 55 nm (half of the ideal skin depth) will result in a 68% of σ_{Cu} conductivity of pure copper as compared to a perfectly smooth surface and Q_0 will drop to 82%. When the effective conductivity is 1/5 of σ_{Cu} , the surface loss will be greater than 55%. The submillimeter interaction circuit requires a machining tolerance from a few to tens of microns. It is a great challenge to manufacture using conventional machining techniques due to the limitation of the tool sizes. To overcome this problem, some advanced approaches have been developed in recent years such as Ultra Violet Lithographic, Galvanik, and Abformung (UV-LIGA), Deep Reactive Ion Etching (DRIE) with copper plating, Wire Electrical Discharge Machining (WEDM), and Nano-computer numerical control (Nano-CNC) machining, which all have made dramatic progress in micro-fabrication [33, 34]. The measured surface roughness is $\sim 30 \text{ nm}$ using UV-LIGA at 220 GHz [35]. Surface roughness of 100 nm was achieved using Nano-CNC machining technology at 263 GHz [34].

CST Microwave Studio was employed to study the effects of tolerance of the circuit parameters on the performance of whole interaction circuit. It was found that the most sensitive geometry is the interaction gap in the cavity especially the

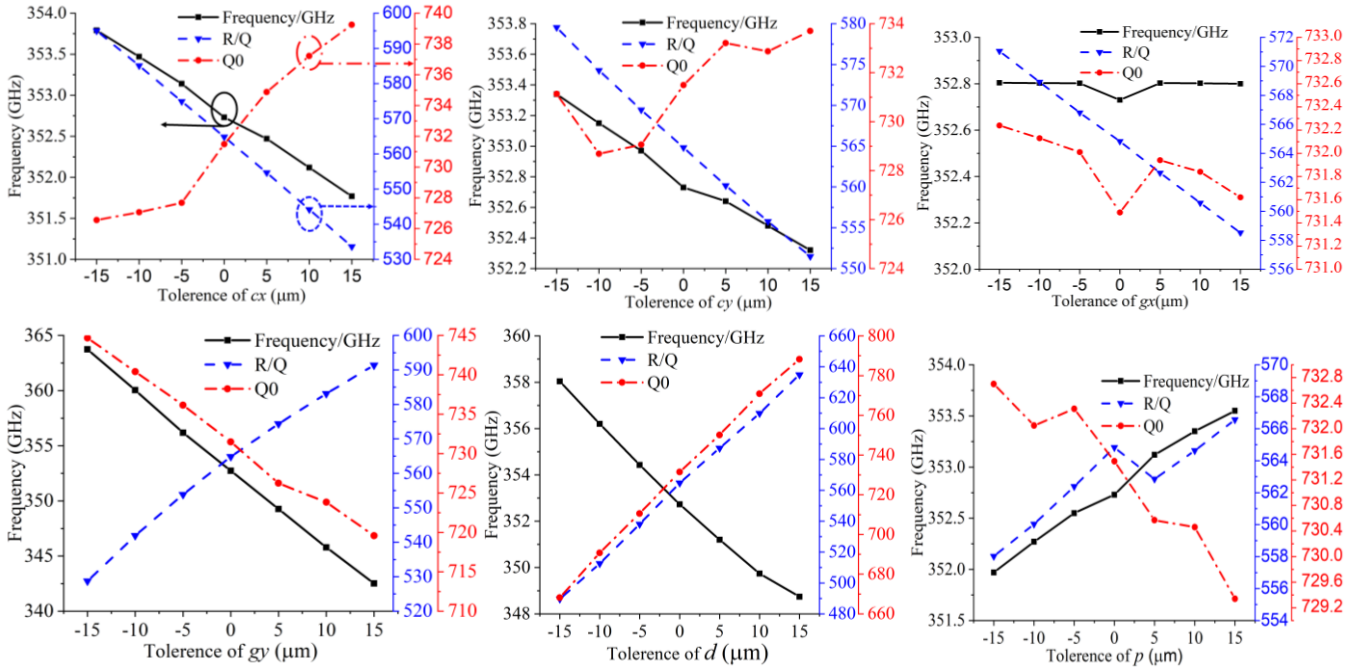


Fig. 6. Tolerance study on the dimensions of the studied EIO structure.

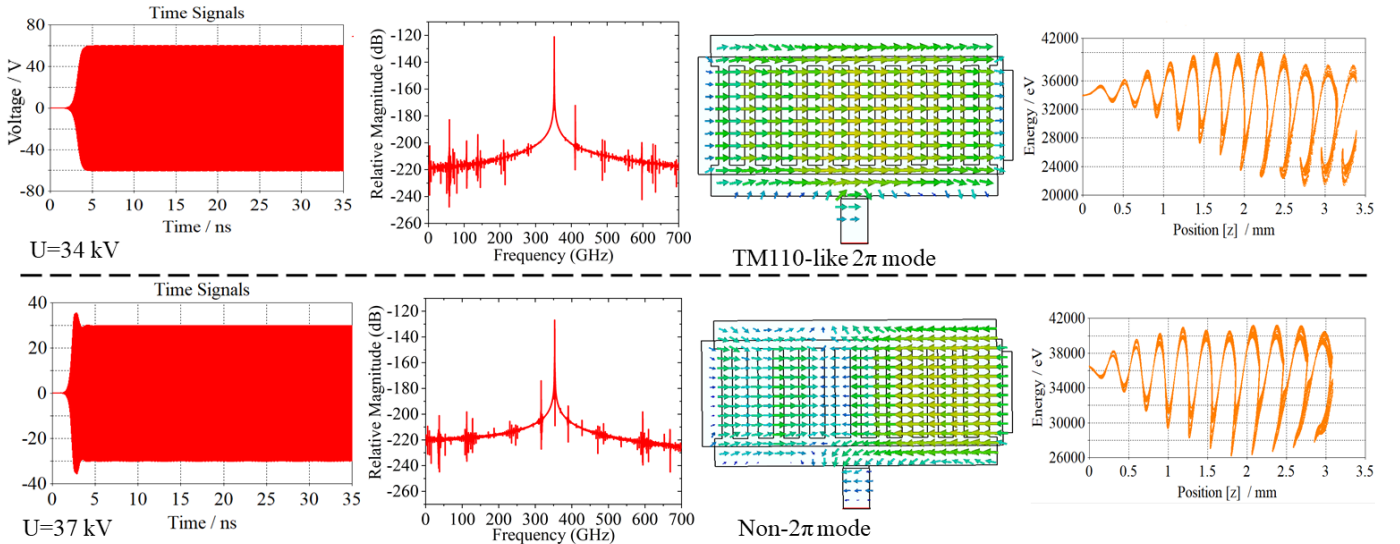


Fig. 7. CST Particle Studio simulation results: output voltage signal, frequency spectrum, electric field distribution, and phase space plots of electrons variation with the operating voltage $U=34$ kV (upside), and $U=37$ kV (underside).

width of gap d and the height of gap g_y . The frequency, Q_0 and R/Q offsets are all far less than 1% with a $\pm 5 \mu\text{m}$ tolerance of c_y , g_x and p . The frequency and Q_0 offsets are all far less than 1% and R/Q offset is about 1.8% with a $\pm 5 \mu\text{m}$ tolerance of c_x . The value of characteristic impedance R/Q increases with the larger the tolerance of d and g_y as shown in Fig. 6. The R/Q offset is about 4% and 1.9% respectively under a $\pm 5 \mu\text{m}$ tolerance of d and g_y . The value of the unloaded quality factor Q_0 also increases as the tolerance of d grows and decreases as the tolerance of g_y increases. The Q_0 offset is about 2.5% and 0.6%, respectively, with a $\pm 5 \mu\text{m}$ tolerance of d and g_y . The characteristic impedance and Q_0 of the cavity are not very sensitive to the changes in g_y . The resonant frequency decreases as the tolerance of d and g_y increases. With a tolerance up to $\pm 5 \mu\text{m}$ of d and g_y , the frequency shift is about 1.5 GHz and 3.5 GHz, respectively. The general definition of Q_0 is $Q_0 = \omega_0 W / P_i$.

Here, the ω_0 is resonant frequency, W is the average energy stored in the resonant cavity and P_i is the power loss in the resonant cavity. In a resonant cavity, a larger Q_0 helps to build the oscillation, and shorten the start-up time. Since the PS discharge produces an electron beam with a short pulse length, a higher Q_0 is of great importance for VEDs based on a PS-sourced electron beam. In our design, a high Q_0 is optimized to ensure a short start oscillation time. Therefore, a fabrication technology that is able to achieve tolerance less than $5 \mu\text{m}$ is preferred, for example, UV-LIGA and high precision CNC machining [35].

B. PIC Simulation and Analysis

3D PIC simulations of the beam-wave interaction were used to validate the design of the planar EIO using CST Particle Studio. A beam current of 6 A (with respect to $5 \times 10^7 \text{ A/m}^2$

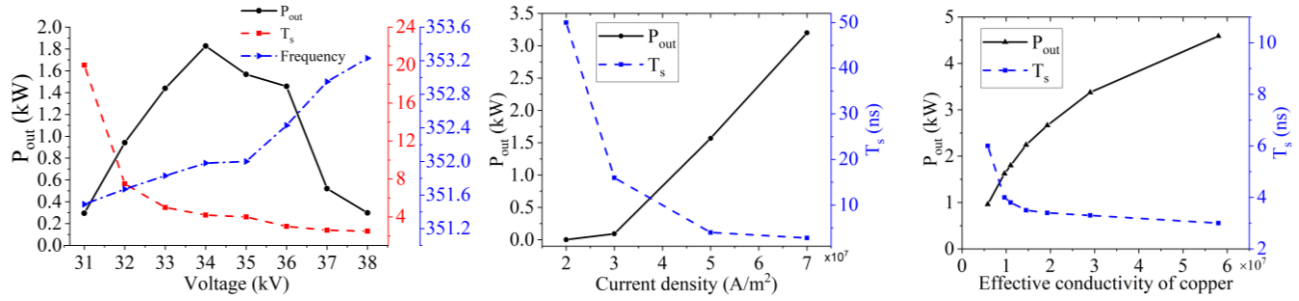


Fig. 8. Simulation results considering some actual situation. (a) P_{out} , T_s and Frequency versus voltage, (b) P_{out} and T_s versus current, and (c) P_{out} and T_s versus effective conductivity of copper.

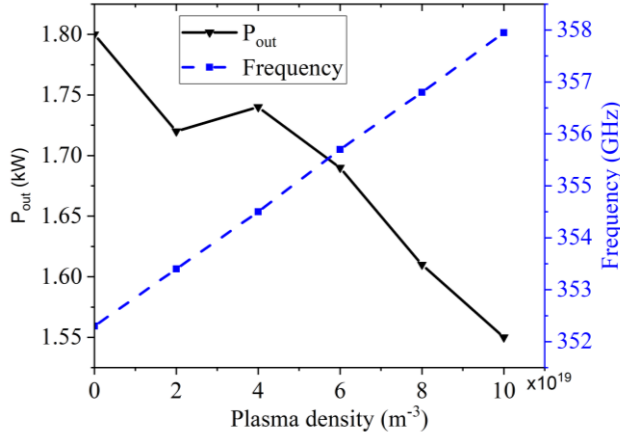


Fig. 9. The effects of plasma density on the output power and frequency.

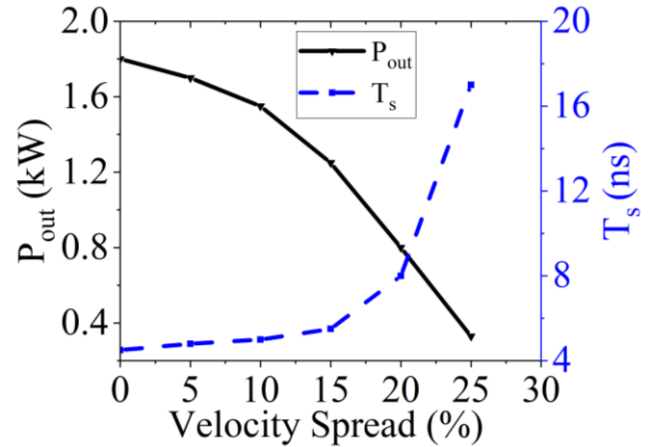


Fig. 10. The effects of velocity spread on the output power and oscillation start-up time.

beam current density) with the voltage of 34 kV is injected into the interaction circuit considering the electrons interception and collision. The conductivity of the background material was set at 1.1×10^7 S/m ($< \sigma_{Cu}/5$) taking into consideration the Ohmic loss. The results are shown in Fig. 7 (up), where obvious bunching and high frequency power extraction is observed. As depicted in Fig. 7 (up), a stable output signal with 60 V (equivalent to output power (P_{out}) of 1.8 kW) was observed at the output port. The center frequency is 352 GHz, which agrees well with the cold analysis (352.4 GHz). The oscillation start-up time T_s (the time required to reach saturated output-power) is about 4.3 ns, which is much smaller than the duration of the PS discharge. As shown in Fig. 7 (down), a non- 2π mode was observed in the electric field distribution, when U is more than 37 kV. The simulated effects of the beam voltages on the P_{out} and oscillation start-up time, as well as the frequency of the output signal, are shown in Fig. 8 (a). When the beam voltage deviates from the optimum operating voltage, the P_{out} drops dramatically due to the drift from the optimal interaction mode (2π mode), which agrees well with the above theoretical analysis of the SWS's dispersion curve. The circuit will operate at the non- 2π mode resulting in a dramatic decrease in P_{out} , when the operation voltage exceeds 37 kV as shown at the bottom of Fig. 7. The oscillation frequency stays around 352 GHz when the voltage is in the range of 32-36 kV. The 3 dB bandwidth is about 0.8 GHz. With the increase of the current density, the P_{out} would increase and the starting time decrease as shown in Fig. 8 (b). When the current density is lower than 3×10^7 A/m², the time required for oscillation build-up would exceed the PS discharge time. The effects of the conductivity of the copper on the P_{out} and oscillation startup time were also

simulated and are shown in Fig. 8 (c). The P_{out} would decrease dramatically with decreasing conductivity. However, even for a background material conductivity of $\sigma_{Cu}/10$ (0.58×10^7 S/m), a P_{out} of 960 W is still predicted. Excellent surface roughness can effectively reduce the deterioration of conductivity due to the high-frequency Ohmic loss of the material as analyzed in part A of section III.

For a microwave device driven by a PS-sourced electron beam, plasma is formed due to the ionization of the background gas. The dispersion curve of the SWS structure will be shifted if the plasma density is high enough [10]. Assuming that the plasma background is uniformly distributed in the SWS, it can be considered as a dielectric media with an equivalent relative dielectric constant of $\epsilon_r = 1 - (\omega_{pe}/\omega)^2$, where $\omega_{pe} = (e^2 n_e / \epsilon_0 m_e)^{1/2}$ is the plasma oscillation frequency, n_e is the electron density in the plasma and m_e is the mass of electron. In the experiment, the plasma density of PS discharge is in the order of 10^{19} to 10^{20} m⁻³ [10]. Therefore, the plasma frequency is in the range of 28 GHz to 90 GHz. The frequency shift due to the plasma is more significant for the interaction circuit operating at a lower frequency, but has less impact for the EIO designed at 352 GHz. Simulations that take into account the background plasma confirm that the frequency of output signal experiences an upshift with the increase of plasma density and the P_{out} decreases as shown in Fig. 9. When the plasma density is 10^{20} m⁻³, the frequency shifts by $\sim 1.7\%$.

The energy spread is an issue of the PS-SEB due to the discharge process and transportation in plasma. Further simulations were carried out to predict the actual situation considering the energy spread. The output power of 330 W is predicted when an energy spread of 25% was used as shown in

Fig. 10. The P_{out} decreases dramatically with increasing energy spread, and the T_s also would be longer. The energy spread of PS-sourced electron beam can be reduced by using the post-acceleration technique [16, 29, 36].

IV. CONCLUSION

This paper presents the design of a PS-SEB EIO operating at 352 GHz which combines the advantages of the SEB and high intense current density of the PS, as well as the high coupling impedance of an EIO interaction circuit, aiming to achieve a compact sub-THz radiation source with high radiation power. Based on the analysis of potential tolerance in the process of fabrication, the influences of tolerance on the circuit performance was studied. The tolerance of $\pm 5 \mu\text{m}$ allowed an acceptable performance to be achieved. The Ohmic loss, which is a significant issue for the THz VED was also studied. The surface roughness caused by the manufacturing technique used would seriously affect the performance of the device due to the surface loss. If the density of the plasma generated from the PS discharge process is high enough, it will affect the resonance frequency of the interaction circuit. The simulations showed that the frequency of the output signal was slightly upshifted, and the output power reduced as the plasma density. At a plasma density of 10^{20} m^{-3} , the frequency would upshift by $\sim 1.7\%$. The PIC simulation results showed that an EIO with 11-period cavities driven by a PS-sourced sheet electron beam can generate a radiation power of up to 1.8 kW at 352 GHz when the background material was set at $1.1 \times 10^7 \text{ S/m}$. The designed PS-SEB EIO will be experimentally studied to verify the simulation results.

REFERENCES

- [1] J. H. Booske *et al.*, "Vacuum Electronic High Power Terahertz Sources," *IEEE Transactions on Terahertz Science and Technology*, vol. 1, no. 1, pp. 54-75, 2011. DOI: 10.1109/THZ.2011.2151610.
- [2] S. S. Dhillon *et al.*, "The 2017 terahertz science and technology roadmap," *Journal of Physics D-Applied Physics*, vol. 50, no. 4, Feb. 2017. DOI: 10.1088/1361-6463/50/4/043001.
- [3] P. H. Siegel, "Terahertz technology," *IEEE Transactions on Microwave Theory and Techniques*, vol. 50, no. 3, pp. 910-928, Mar. 2002. DOI: 10.1109/22.989974.
- [4] J. X. Qiu *et al.*, "Vacuum Tube Amplifiers," *IEEE Microwave Magazine*, vol. 10, no. 7, pp. 38-51, Dec. 2009. DOI: 10.1109/MMM.2009.934517.
- [5] N. Kumar, U. Singh, T. P. Singh, and A. K. Sinha, "A Review on the Applications of High Power, High Frequency Microwave Source: Gyrotron," *Journal of Fusion Energy*, vol. 30, no. 4, pp. 257-276, Aug. 2011. DOI: 10.1007/s10894-010-9373-0.
- [6] R. K. Parker, R. H. Abrams, B. G. Danly, and B. Levush, "Vacuum electronics," *IEEE Transactions on Microwave Theory and Techniques*, vol. 50, no. 3, pp. 835-845, Mar. 2002. DOI: 10.1109/22.989967.
- [7] R. L. Ives *et al.*, "High Current Density, Reservoir Cathodes for High Frequency Applications," *35th International Conference on Infrared, Millimeter, and Terahertz Waves (IRWMM-Thz 2010)*, 2010.
- [8] J. Zhao *et al.*, "Scandate Dispenser Cathode Fabrication for A High-Aspect-Ratio High-Current-Density Sheet Beam Electron Gun," *IEEE Transactions on Electron Devices*, vol. 59, no. 6, pp. 1792-1798, 2012. DOI: 10.1109/ED.2012.2190294.
- [9] H. Yin *et al.*, "Millimeter wave generation from a pseudospark-sourced electron beam," *Physics of Plasmas*, vol. 16, no. 6, June 2009. DOI: 10.1063/1.3155444.
- [10] W. He *et al.*, "Generation of broadband terahertz radiation using a backward wave oscillator and pseudospark-sourced electron beam," *Applied Physics Letters*, vol. 107, no. 13, Sep. 28 2015. DOI: 10.1063/1.4932099.
- [11] G. X. Shu *et al.*, "Demonstration of a Planar W-Band, kW-Level Extended Interaction Oscillator Based on a Pseudospark-Sourced Sheet Electron Beam," *IEEE Electron Device Letters*, vol. 39, no. 3, pp. 432-435, Mar. 2018. DOI: 10.1109/LED.2018.2794469.
- [12] H. Yin *et al.*, "Compact high-power millimetre wave sources driven by pseudospark-sourced electron beams," *IET Microwaves, Antennas & Propagation*. doi: 10.1049/iet-map.2018.6190 Available: <https://digital-library.theiet.org/content/journals/10.1049/iet-map.2018.6190>
- [13] H. Yin, A. W. Cross, W. He, A. D. R. Phelps, and K. Ronald, "Pseudospark experiments: Cherenkov interaction and electron beam post-acceleration," *IEEE Transactions on Plasma Science*, vol. 32, no. 1, pp. 233-239, Feb. 2004. DOI: 10.1109/Tps.2004.823986.
- [14] N. Kumar, R. P. Lamba, A. M. Hossain, U. N. Pal, A. D. R. Phelps, and R. Prakash, "A tapered multi-gap multi-aperture pseudospark-sourced electron gun based X-band slow wave oscillator," *Applied Physics Letters*, vol. 111, no. 21, Nov. 2017. DOI: 10.1063/1.5004227.
- [15] Y. Yin, W. L. He, L. Zhang, H. B. Yin, C. W. Robertson, and A. W. Cross, "Simulation and Experiments of a W-Band Extended Interaction Oscillator Based on a Pseudospark-Sourced Electron Beam," *IEEE Transactions on Electron Devices*, vol. 63, no. 1, pp. 512-516, Jan. 2016. DOI: 10.1109/TED.2015.2502950.
- [16] J. Zhao *et al.*, "Experiments on W-band extended interaction oscillator with pseudospark sourced post-accelerated electron beam," *Physics of Plasmas*, vol. 24, no. 6, Jun 2017. DOI: 10.1063/1.4985684.
- [17] G. X. Shu *et al.*, "Experimental demonstration of a terahertz extended interaction oscillator driven by a pseudospark-sourced sheet electron beam," *Applied Physics Letters*, vol. 112, no. 3, Jan. 2018. DOI: 10.1063/1.5011102.
- [18] J. Xie *et al.*, "Theoretical study of extended interaction frequency-locking oscillator based on carbon nanotube cold cathodes," *IET Microwaves Antennas & Propagation*, vol. 12, no. 11, pp. 1771-1774, Sep. 2018. DOI: 10.1049/iet-map.2018.5509.
- [19] A. Roitman, D. Berry, and B. Steer, "State-of-the-art W-band extended interaction klystron for the CloudSat program," *IEEE Transactions on Electron Devices*, vol. 52, no. 5, pp. 895-898, May. 2005. DOI: 10.1109/TED.2005.845799.
- [20] D. Berry *et al.*, "Practical Aspects of EIK Technology," *IEEE Transactions on Electron Devices*, vol. 61, no. 6, pp. 1830-1835, 2014. DOI: 10.1109/TEDE.2014.2302741.
- [21] B. Steer, A. Roitman, P. Horoyski, M. Hyttinen, R. Dobbs, and D. Berry, "Advantages of Extended Interaction Klystron technology at millimeter and sub-millimeter frequencies," *2007 IEEE Pulsed Power Conference, Vols 1-4*, pp. 1049-1053, 2007. DOI: 10.1109/PPPS.2007.4652369.
- [22] J. Christiansen and C. Schultheiss, "Production OF High-current Particle Beams by Low-pressure Spark Discharges," *Zeitschrift Fur Physik a-Hadrons and Nuclei*, vol. 290, no. 1, pp. 35-41, 1979. DOI: 10.1007/bf01408477.
- [23] H. Yin, A. W. Cross, A. D. R. Phelps, W. He, and K. Ronald, "Cherenkov interaction and post-acceleration experiments of high brightness electron beams from a pseudospark discharge," *Nuclear Instruments & Methods in Physics Research Section A-Accelerators Spectrometers Detectors and Associated Equipment*, vol. 528, no. 1-2, pp. 378-381, Aug. 2004. DOI: 10.1016/j.nima.2004.04.084.
- [24] A. W. Cross, H. Yin, W. He, K. Ronald, A. D. R. Phelps, and L. C. Pitchford, "Generation and application of pseudospark-sourced electron beams," *Journal of Physics D-Applied Physics*, vol. 40, no. 7, pp. 1953-1956, Apr. 7 2007. DOI: 10.1088/0022-3727/40/7/018.
- [25] J. B. Zhu, M. C. Wang, Z. J. Wang, and J. K. Lee, "Design of high-voltage and high-brightness pseudospark-produced electron beam source for a Raman free-electron laser," *Optical Engineering*, vol. 35, no. 2, pp. 498-501, Feb. 1996. DOI: Doi 10.1117/1.600922.
- [26] H. Yin, G. R. M. Robb, W. He, A. D. R. Phelps, A. W. Cross, and K. Ronald, "Pseudospark-based electron beam and Cherenkov maser experiments," *Physics of Plasmas*, vol. 7, no. 12, pp. 5195-5205, Dec. 2000. DOI: Doi 10.1063/1.1319637.
- [27] Varun and U. N. Pal, "PIC Simulation to Analyze Peak Electron Current Generation in a Triggered Pseudospark Discharge-Based Plasma Cathode Electron Source," *IEEE Transactions on Electron Devices*, vol. 65, no. 4, pp. 1542-1549, Apr. 2018. DOI: 10.1109/TED.2018.2808175.
- [28] N. Kumar *et al.*, "Experimental Analysis of Pseudospark Sourced Electron Beam," *Journal of Infrared Millimeter and Terahertz Waves*, vol. 32, no. 12, pp. 1415-1423, Dec 2011. DOI: 10.1007/s10762-011-9830-5.
- [29] H. Yin, A. W. Cross, A. D. R. Phelps, D. Zhu, W. He, and K. Ronald, "Propagation and post-acceleration of a pseudospark-sourced electron

- beam," *Journal of Applied Physics*, vol. 91, no. 8, pp. 5419-5422, Apr. 2002. DOI: 10.1063/1.1459757.
- [30] M. Chodorow and T. Wessel-Berg, "A high-efficiency klystron with distributed interaction," *IRE Transactions on Electron Devices*, vol. 8, no. 1, pp. 44-55, 1961. DOI: 10.1109/T-ED.1961.14708.
- [31] A. Gilmour, *Klystrons, traveling wave tubes, magnetrons, crossed-field amplifiers, and gyrotrons*. Norwood, MA: Artech House, 2011.
- [32] M. Kirley and J. H. Booske, "Terahertz conductivity of copper surfaces," *IEEE Transactions on Terahertz Science and Technology*, vol. 5, no. 6, pp. 1012-1020, 2015. DOI: 10.1109/TTHZ.2015.2468074.
- [33] Y. M. Shin *et al.*, "Microfabricated THz Sheet Beam Vacuum Electron Devices," *2011 36th International Conference on Infrared, Millimeter, and Terahertz Waves (IRMMW-THz)*, 2011. DOI: 10.1109/irmmw-THz.2011.6105031.
- [34] D. Gamzina *et al.*, "Nano-CNC Machining of Sub-THz Vacuum Electron Devices," *IEEE Transactions on Electron Devices*, vol. 63, no. 10, pp. 4067-4073, Oct. 2016. DOI: 10.1109/Ted.2016.2594027.
- [35] Y. M. Shin, J. F. Zhao, A. Baig, D. Gamzina, L. R. Barnett, and N. C. Luhmann, "Micro-Fabricable Terahertz Sheet Beam Amplifier Integrated with Broadband Metamaterial Circuit," *2010 Third International Conference on Communications and Electronics (ICCE)*, pp. 373-378, 2010. DOI: 10.1109/ICCE.2010.5670649.
- [36] J. Zhao *et al.*, "Advanced post-acceleration methodology for pseudospark-sourced electron beam," *Physics of Plasmas*, vol. 24, no. 2, Feb. 2017. DOI: 10.1063/1.4975188.